ISABE-2015-20056

UNSTEADY INVESTIGATION ON TIP FLOW FIELD IN COUNTER-ROTATING AXIAL COMPRESSOR AT STALL INCEPTION CONDITION

Limin Gao[1,2], Ruiyu Li[1,2], Fang Miao[1], Yutong Cai[1,2]
School of Power and Energy, Northwestern Polytechnical University, 710072 Xi'an, China
Collaborative Innovation Center of Advanced Aero-engine
Beijing, 100191, P.R. China

ABSTRACT

Counter-rotating axial compressor (CRAC) is a promising technology to meet the future requirement of the aircraft industry. Massive time accurate simulations are performed to investigate rotating stall in CRAC comprised of two counter-rotating rotors. Particularly, the back pressure is increased with very small step to capture accurately the flow field transition from stability to instability. Due to the nonexistence of stator, the instability of downstream rotor is stronger. The present studies mostly focus on the downstream rotor. The tip leakage flow field is analyzed in detail under near-stall condition, which indicates that a secondary leakage flow plays an important role to cause the CRAC's unsteady flow field. The frequency analysis in the tip clearance of downstream rotor has been made under multiple near stall conditions, and the transition of the second harmonic frequency is captured, which can be used as stall inception signal. Moreover, the rotating stall onset process in real CRAC is simulated numerically.

Introduction

Owing to unique design of counter-rotating technology, Contra-Rotating Axial flow Compressor/Fan (CRAC) has been considered as a promising technology to meet the future goals aircraft industry [1]. CRAC wherein the stator between two rotors is canceled and two adjacent rotors rotate in the opposite direction will not only bring some benefits from higher pressure ratio, but also lower the weight of the engine. The above benefits of counter-rotation have been known since the 1950's[2], and some investigations have been done in Massachusetts Institute of Technology (MIT) [3], the German Aerospace Center (DLR)[4], and Northwestern Polytechnical University[5,6]. Recently, its potentiality has been validated further by its successful utilization in VTOL (Vertical Take-off and Landing) aircraft as the contra-rotating lift fan fixed on F35-B and the large transport plane An-70 as the counter-rotating fan developed by Russian and Ukraine together.

So far as studies on CRAC concerned, most researches focus on total performance. Mark G. Turner et al [7] have numerically studied the aspirated counter-rotating compressor in MIT. A comparison between the aspirated and non-aspirated simulations shows the total performance improvement in aspirated case. Robert Meyer et.al[8] of the German Aerospace Center (DLR) has measured the unsteady flow of a high speed Contra-Rotating Turbo Fan by using hot-ware measurements, and they focus on noise and efficiency prediction. In China, after the first high speed CRAC test rig was completed, Liu Bo et al have done various researches into aerodynamic characteristics[9-10]. However, the aerodynamic stability is also indispensable. Researchers have made tremendous progress on investigating the flow phenomenon and the mechanisms of rotating stall in axial compressor 11-13. While the questions about stalling characteristic of the CRAC and the stalling characteristic difference between a CRAC and a general compressor are still open. These

questions motivate us study the stability of the CRAC. GAO Limin et al[14-16] have made many investigations on the CRAC test rig in Northwestern Polytechnical University, and the results show that downstream rotor firstly presents stall instability at near stall condition under design rotating speed and tip clearance, and the effect of different rotating speed ratios and tip clearance size in rotating stall stages are analyzed in succession .

Description of the CRAC

The research object of this paper is a dual-stage CRAC rig in Northwestern Polytechnical University. It consists of a clockwise-rotating first rotor (ROT1) and an anti-clockwise-rotating second rotor (ROT2) with hub-to-tip ratio of 0.61 and 0.63, respectively. Besides, CRAC produces a total pressure ratio of 1.22 and an adiabatic efficiency of 89% at a mass flow rate of 6.4 kg/sec at the design speed of 8000 RPM. Design speed ratio is chosen only for the sake of simplification and does not represent the optimum selection. Table1 lists some of the specific parameters of them. Detailed description of the CRAC can be seen in literature[17].

Table.1 Parameters of CRAC

	ROT1	ROT2
Blade number	19	20
Hub-tip ratio	0.485	0.641
Tip clearance	0.5 mm	0.5mm
Design speed	8000 rpm	-8000 rpm

Simulation Method

A Numerical Approach

EURANUS solver is used to solve the compressible Reynolds-averaged Navier-Stokes equations, which is integrated in the software FINE/Turbo. Spalart-Allmaras (S-A) turbulence model is selected to compute the turbulent viscosity, which has been validated in the previous research on CRAC[20]. Unsteady simulation is based on the implicit dual-time stepping technique and every instantaneous flow solution is considered as a "pseudo-steady" problem in which an explicit four-stage Runge-Kutta scheme with local time step is used. 20 physical time steps per blade passage and 40 inner iterations per time step are performed for the present study.

B Computational Grids

To reduce the numerical simulation cost, computational model is simplified. The geometry characteristic of the upstream rotor is performed by the method of domain scaling, and blade number is changed from 19 to 20 under the principle of keeping solidity invariant. Finally, blade number of two rotors becomes the same as 20, and periodical boundary condition is applied, so only partial passage rather than the full annulus will be simulated.

The computational mesh is generated by the pre-processing mesh generator module Autogrid5. Type of structured HOH topology is generated for each blade passage. The shroud gap of each stage is modeled using a butterfly grid topology (Fig.1(a)). The ratio of the minimum grid spacing on solid walls is less than 5×10^{-6}m to evaluate the viscous fluxes at the walls. This minimum grid spacing gives $y^+ < 5$ at the walls, which is satisfied with the requirement of the S-A turbulence model. A grid independence study[14] is performed to obtain proper mesh.

Restricted by computation resource, investigations on flow unsteadiness are based on single rotor passage and on stall mechanism is performed in five passages under the stall inception, which is according to the characteristic of the spike stall inception[18]. Finally, the whole grid system has more than 7.13 million cells, and Fig.1(b) depicts the computational geometry and grid distributions on the rotor blades and the hub schematic.

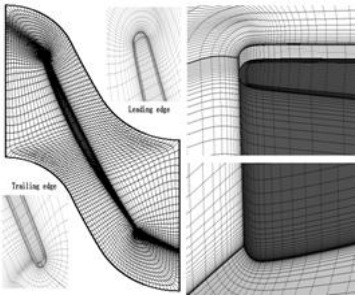

(b) Grids of the rotor

(b) Three-dimensional computing grid

Figure 1. Computing grids

Rotating stall margin of CRAC is captured by the outlet back pressure increasing. When the work condition is far from the stall marge, the back pressure is improved with the step of 200Pa, but the pressure step is shorten as 50Pa around the stall condition so as to avoid missing flow field transition from stability to instability. The results of numerical simulation are shown in Fig.2 (a). Partial performance under the small mass rate is enlarged as Fig.2 (b), which is labeled as point A, B, C, D and E. These are the major conditions analyzed in the next sections. Detailed computational sets and results under each condition are given in Table2.

C Computational Schemes

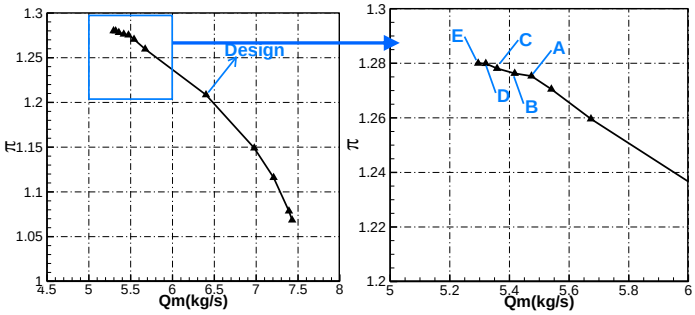

(a) Pressure ratio performance (b) Partial enlarging drawing

Fig.2 Pressure ratio performance

Table2. Parameters under near stall marge

Different Conditions	Computational passages	Outlet pressure	Time averaged mass flow	Time averaged pressure ratio	Second harmonic
Design	Single	117514Pa	6.4kg/s	1.212	0
Condition A	Single	124800Pa	5.48kg/s	1.275	0.64BPF
Condition B	Single	125000Pa	5.41kg/s	1.276	0.64BPF
Condition C	Single	125200Pa	5.36kg/s	1.278	1.5BPF
Condition D	Five	125400Pa	5.32kg/s	1.279	1.5BPF
Condition E	Five	125450Pa	5.29kg/s	1.280	1.5BPF

Analysis of the Numerical Results

A. Tip Leakage Flow Analysis under Condition B

To preliminary understand the tip clearance leakage flow, the flow field in tip clearance is analyzed under condition B because it is near the stall marge while still relatively stable.

Dimensionless parameters Su[19] is used to measure quantitatively the unsteadiness intensity in a periodic unsteady flow field, which is defined as follows:

$$Su(z,r,\theta)=\sqrt{\frac{1}{T}\int_{t_1}^{t_1+T}\left[f(z,r,\theta,t)-\overline{f}(z,r,\theta)\right]^2 dt} \quad (2)$$

where, f is the instantaneous value of a flow variable and $\overline{f}$ is its corresponding time-averaged

component. *T* represents the time period of the unsteady periodic flow field and is computed from the blade passing time through its neighbor blade row. The pressure fluctuation intensity in the tip clearance of two rotors is presented in Fig.3. Due to working at the positive attacking angle condition of inlet distortion, the value of *Su* is larger in ROT2's blade passage than in ROT1's, which means the unsteadiness in ROT2 is stronger than in ROT1, so the following unsteadiness analysis of the tip leakage flow is focused near stall condition.

Due to near the stall condition, it seems to the streamline in the tip clearance of ROT2 is disordered as shown in Fig.5 (a). However, it is observed carefully that the leakage can be decomposed into two parts. Some upstream flow near the blade tip enters the channel between two adjacent blades as shown in Fig.5(b), which is the main leakage part, because the circumferential change of the static pressure is weak for the absence of the rotor blade. The other flow near the casing across the next blade tip one after another but not entering the channel directly, and it is circled by the black line in Fig.5(c). It is the secondary leakage. Due to the relative movement of the casing and the viscous fluid, the circumferential pressure gradient in the tip clearance increases from the blade tip to the casing which can be also verified in Fig.4. It means the occurrence of secondary leakage results from the larger pressure difference between two blade sides. It is also found that the secondary leakage occurs when the operating condition approaches to the stall margin.

Combined with the position of the strongest unsteadiness in ROT2's blade passage (shown in Fig.3), the spill leakage flow crashes to the leading edge in Fig.5(c) leading to the unsteadiness of the secondary leakage flow.

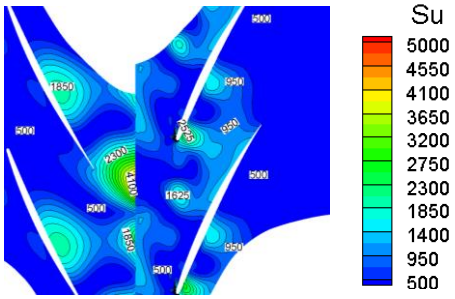

Fig.3 Unsteadiness intensity at 99% span of compressor

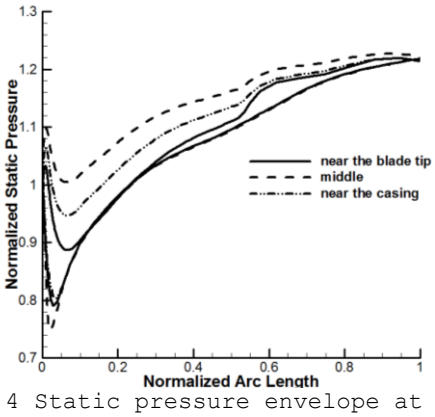

Fig.4 Static pressure envelope at different height in tip clearance

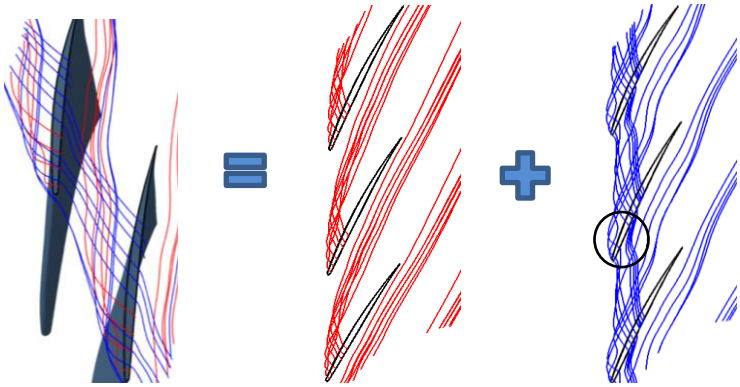

(a)Tip leakage flow (b) Main leakage flow (c) Secondary leakage flow

Fig.5 Tip leakage flow

B. Stall Inception Analysis

FFT analysis of static pressure on ROT2 tip under Condition B is given in Fig.6 which is monitored

by numerical probes at the leading edge (L.E.), middle (M.E.) and trailing edge (T.E.). At each position, 2BPF (Blade Passing Frequency), but 0.64BPF and its multiple frequencies exist. Interestingly, the amplitude of 2BPF fluctuation rapidly increases along the chord direction and reaches its maximum around the trailing edge. But the trend of amplitude variation of 0.64BPF is opposite and seems to peak at the leading edge. Along the span in Fig.7, 2BPF fluctuation on ROT2 50% of span is stronger than that on the tip (Fig.6) but the amplitude of 0.64BPF is too weak even to be ignored. Thus 0.64BPF is deduced that the fluctuation of the secondary leakage flow spills at the leading edge.

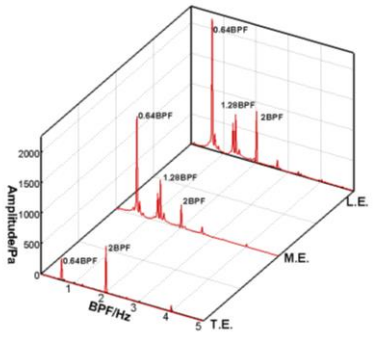

Fig.6 FFT analysis of static pressure on ROT2 tip under Condition B

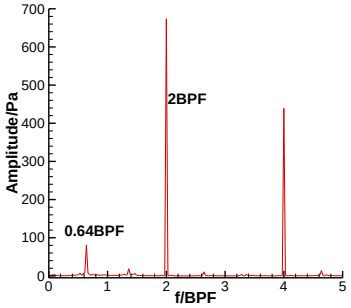

Fig.7 FFT analysis of static pressure at the leading edge on ROT2 50% span

To analysis the effect of the working condition on the unsteady fluctuation, FFT analysis of outlet mass flow under the design and other conditions are showed in Fig.8. Under all working conditions, 2BPF fluctuation dominates the unsteady flow field in ROT2, which is just the result of the relative motion between two rotors, and strengthens with the mass flow decreasing. Noticeably, a second harmonic of 0.64BPF occurs under Condition A and increases further under Condition B. But it nearly disappears under Condition C and the second harmonic of 1.5BPF grows up unexpectedly, which means the more secondary leakage flow and the quicker spill. Frequencies of the second harmonic under other working conditions are also given in Table2.

In summary, a second leakage flow spilling along the leading edge on ROT2 tip appears and plays an important role on the CRAC's unsteady flow field when the CRAC operating condition is close to the stall margin. The appearance of 0.64BPF second harmonic is therefore used to predict the stall inception and the frequency transition from 0.64BPF to 1.5BPF is used as the rotating stall warning.

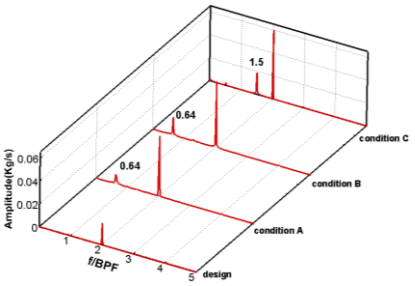

Fig.8 FFT analysis of outlet mass flow under different condition

C. Stall Onset Analysis

Based on Condition D, the pressure step is set as 50 Pa, which is enough small to study on the rotating stall. From Fig.9, both flow field under Condition D and Condition E are still stable because of their periodic iterating histories. As the back pressure is increased with the 50Pa on the basis of Condition E, the mass flow decreased quickly with the time marching which is named as Condition S in Fig.9. It should be explained that, the unsteady computation in Fig.9 is performed after T=0 and the previous is the steady computation.

Although the simulation of Condition S is an invalid computation theoretically, the unsteady flow field under Condition S can be used for the stall mechanism exploration of

CRAC, considering the difficulty and limitation of experiment.

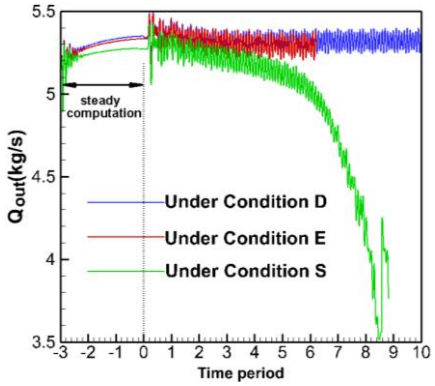

Fig.9 Comparison of mass-iteration histories

The instantaneous flow field at T=3 is shown in Fig.10. There is an obvious interface between the high entropy zone and the low in front of both rotors, however, the periodicity of flow field on the tip region is still kept in ROT1 but disappear in ROT2: the maximum entropy locates at the front half passage of both passage 3 and 4, and the second leakage flow spills near ROT2's leading edge with different spillage. Under the movement of the clockwise vortex in the middle of the passage 5, the outflow near the suction surface is rolled towards the pressure surface but not the downstream, then turns around the trailing edge and enters the adjacent passage 4, which forms the trailing edge backflow. In the passage 4, a part of the backflow spills at the leading edge on the pressure side which further forms the second leakage flow and aggravates the flow field. According to Vo[24], both the trailing edge backflow and the leading edge spillage in CRAC's tip clearance agree well with the characteristic of the spike stall inception.

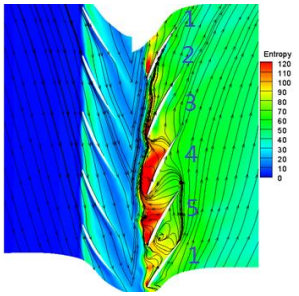

Fig.10 Tip region flow field at T=3

With time marching, the flow field degenerates further. At the 8th time period (T=8), the most serious blockage moves from the passage 4 to 3 and the interface between the main flow and the tip leakage flowis pushed out of two rotor passages due to the increasing blockage, as seen in Fig.11. The momentum of the main flow is not enough to balance the tip leakage flow and the mass flow entering CRAC. Meanwhile, due to the absent of the stator between two rotors, the upstream periodicity of ROT1 is broken immediately under the action of the potential reverse flow from ROT2.

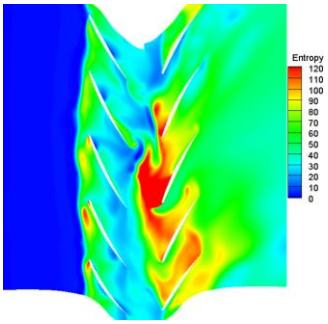

Fig.11 Tip region flow field at T=8

Entropy contour at the 25% of the axial chord length of ROT2 is shown in Fig.12. At T=3 (Fig.12 (a)), there is a high entropy zone occurs at the tip clearance in each passage, especially the passage 1, 2and 3. As time goes on (T=6 and T=7), the high entropy zones is enlarged and moves along the pitchwise (Fig.12(b)) and Fig.12(c)). Noteworthy, at the next time period T=8 in Fig.12(d), the high entropy zone grows up abruptly along the spanwise, even occupies more than 50% height of the passage. The low energy flow in passage 3 and 4 leads to the rotating stall onset of CRAC. From the stall inception to the matured stall cell, the high entropy always exists in three blade passages and the whole process experiences only 5 time periods. The characteristic of the short-time and the small-scale indicates further that there is a spike stall inception in ROT2 of CRAC. Compared with Fig.12, there is no obvious high entropy region in ROT1 except the tip region and is still periodic until T=7, as shown

in Fig.13. It means ROT2 is the first stall stage in CRAC, which is coincided with our previous work[17] using the steady computation.

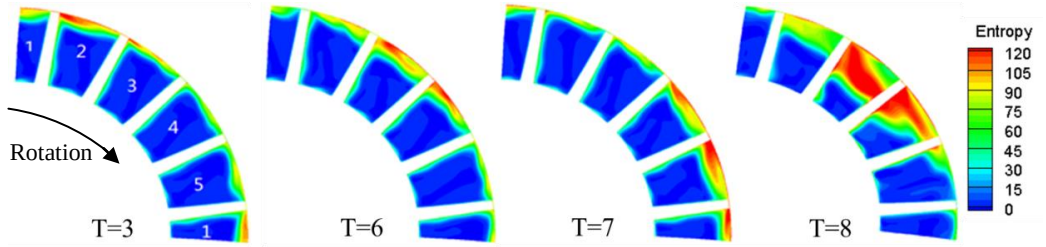

(a) (b) (c) (d)

Fig.12 Entropy contour at 25% axial chord from the blade leading edge of ROT2

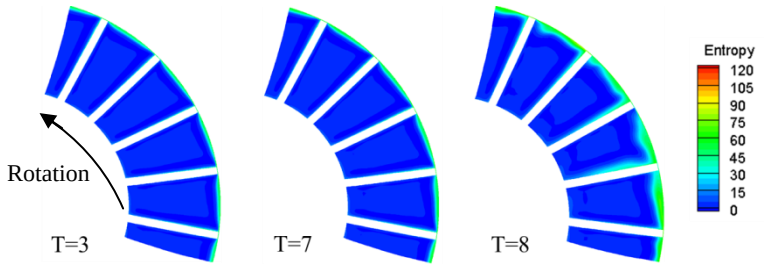

Fig.13 Entropy contour at 25% axial chord from the blade leading edge of ROT1

The flow field in tip region of ROT2 at T=7 is depicted in Fig.14 to further explore the mechanism of rotating stall in CRAC. At this time (T=7), the stall cell is matured from the stall inception, and the stream line pattern is obviously difference in each passage.

In Fig.14 (a), the tip leakage vortex in the passage 1 breaks down and the second leakage flow spills the adjacent passage 5 at the leading edge with the anti-clockwise direction. As shown in Fig.14 (b), the flow field in the passage 2 is dominated by the massive vortex breakdown, which blocks the incoming flow and rolls up further. Eventually, it enters the passage 1 and has an effect on the flow field in the passage 1. In the passage 3 (Fig.14 (c)), it can be seen that the partial flow in passage 3 is rolled by the breakdown vortex in the passage 2 and forms a local back-flow at the trailing edge in passage 2. Then it crosses the tip of blade 1 and spills at the blade5's leading edge. Meanwhile, the vortex core in the passage 3 moves close to the pressure side of the blade2, which means the momentum of the leakage flow is very strong.

As shown in Fig.14(d) and 14 (e), the leakage flow enters the passage 4 and 5 smoothly and the second leakage flow is absent, which means that tip vortex is still stable relatively. Along ROT2 rotating direction, it is visible that the flow in passage 4 leaves from the stall. while due to the influence of the flow field in passage 1 and 2, the flow in passage 5 will meets the next rotating stall.

The breakdown vortex always propagates opposite to the direction of ROT2 rotating. With the further decreasing of the mass flow, the difference of the flow angle will enlarged for every passage. The stable flow will collapse thoroughly and the rotating stall develop in CRAC.

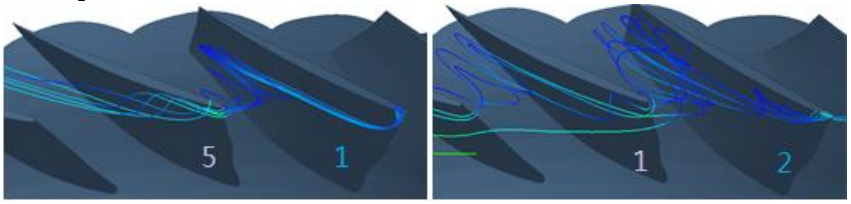

(a) Passage 1 (b) Passage 2

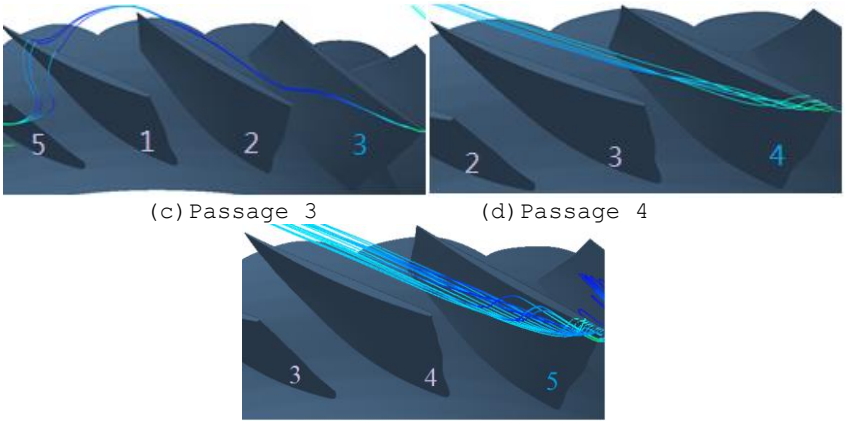

(c) Passage 3 (d) Passage 4

(e) Passage 5

Fig.14 Tip vortex distribution in different passages at T=7

Conclusions

In this paper, time accurate simulations are performed to investigate rotating stall in a dual-row CRAC when stall inception. 20 physical time steps per blade passage and 40 inner iterations per time step are performed for the present study. Besides, Rotating stall margin of CRAC is captured by the back pressure increasing with small steps. Noteworthily, the current study is performed in single rotor passage but the analysis of stall onset is based on five rotor passages.

This study has obtained multiple unsteady flow field data. Investigation on the tip clearance flow in CRAC indicates that the unsteadiness in downstream rotor is stronger as the result of missing stator. The analysis on the ROT2's tip clearance flow field shows that secondary leakage flow has an important influence on the unsteadiness of CRAC, and the transition of second harmonic frequency can be used to incept the rotating stall. Finally, the development of rotating stall in CRAC is simulated successfully at stall onset, and the study demonstrates the breakdown vortex is the main reason for the formation of blockage in downstream rotor's tip region, which is the fundamental origin of the CRAC ultimately stepping into rotating stall.

Acknowledgment

This research is supported by the National Nature Science Foundation of China (NSFC) under the grant number 51076132.

References

[1] Lengyel, T., Voß, C., and Schmidt, T., 2009, "Design of a counter rotating fan-An aircraft engine technology to reduce noise and CO2-emissions," ISABE Conference on Air Breathing Engines, Montreal, Canada,Paper No.ISABE-2009-1267.

[2] Young, R.H., 1951, "Contra-Rotating Axial-Flow Fans," J. Inst. Heat. Ventilat. Eng., 18(187), pp. 448-477.

[3] Knapke, R. D., and Turner, M. G., 2013, "Detailed unsteady simulation of a counter rotating aspirated compressor with a focus on the aspiration slot and plenum," International Journal of Rotating Machinery, ID857616.

[4] Robert, M., Karsten, K., and Johannes, L., 2010, "Hot-wire measurements in a high speed counter rotating turbo fan rig," ASME Paper No.GT2010-22569.

[5] Liu B., Chen Y.Y, and Xiang X.R., 2008, "Experimental and numerical investigation of dual stage counter-rotating compressor," (in Chinese) Journal of Propulsion Technology, 29(4), pp.454-457.

[6] Gao, L., Li, X., and Xie, J., 2012, "The numerical study of the effect of speed ratio on the first rotating stall stage in contra-rotating compressor," ASME Paper No.GT2012-68802.

[7] Knapke R D, Turner M G, Michael G. List, et al. Time accurate

simulations of a counter-rotating aspirated compressor. ASME Paper, GT2008-50877

[8] Meyer R, Knobloch K, Linden J. Hot-wire measurements in a high speed counter rotating turbo fan rig. ASME Paper, GT2010-22569

[9] Chen, Y.Y., Liu, B. and Xiang, X.X., 2008, "A study of speed ratio affecting the performance of a contra-rotating axial compressor", Proceedings of the Institution of Mechanical Engineers, Part G: Journal of Mechanical Engineering Science, 222(7), pp:985-991.

[10] Wang, L., Liu, B., 2012, "Investigation of the unsteady flow in a counter-rotating compressor using the nonlinear harmonic method0", International Journal of Energy Science, 2(5), pp:182-188.

[11] Choi, M., and Vahdati, M., 2011, "Recovery process from rotating stall in a fan," Journal of Propulsion and Power, 27(6), pp.1161-1168.

[12] Vo, H. D., 2010, "Rotating stall suppression in axial compressors with casing plasma actuation," Journal of Propulsion and Power, 26(4), pp.808-818.

[13] Zaki, M., Sankar, L. N., and Menon, S., 2009, "Numerical stall inception predictions for axial compressors using a hybrid RANS/KES turbulence model," AIAA 45th Joint Propulsion Conference and Exhibit, Denver, Colorado, August 2-5, AIAA Paper No. 2009-5374.

[14] Gao, L., Li, X., and Feng, X., 2012, "Investigation of influence of rotational speed ratio on stability boundary of counter-rotating compressor," Journal of Propulsion Technology, 33(6), pp.881-887.

[15] Li,X., Gao, L., and Xie, J., 2012, "Study of rotating stall mechanism of dual-stage contra-rotating compressor," Journal of Aerospace Power, 28(1), pp.188-194.

[16] Gao, L., Li X., and Feng, X., 2012, "The numerical study on the effect of tip clearance size on the performance of counter rotating compressor," ASME Paper No.GT2012- 68801.

[17] Cheng, Y., 2008, "Flow field and performance investigation and three-dimension optimization study of contra-rotating compressor," Ph.D. Thesis, Northwestern Polytechnical University, Xi'an, China.

[18] Day, I. J., 1993, " Stall inception in axial flow compressors," ASME J Turbomach, 115(1), pp. 1-9.

[19] Gao, L., Xi, G., and Zhou, Li., 2005, "Experimental and computational investigation of flows in a vaned diffuser under stage environment," (in Chinese) Acta Mechanica Sinica, 37(1), pp.110-119. .